# Dental Splint Fabrication for Prospective Motion Correction in Ultrahigh-Field MR Imaging

Gabriel Mistelbauer[1], Daniel Stucht[2], Yan L. Arnold[2], Oliver Speck[2], Bernhard Preim[1]

[1]Dept. Simulation and Graphics, Otto-von-Guericke University Magdeburg, Germany
[2]Dept. Biomed. Mag. Resonance, Otto-von-Guericke University Magdeburg, Germany
gmistelbauer@isg.cs.uni-magdeburg.de

**Abstract.** For prospective motion correction in ultrahigh-field magnetic resonance imaging, optical tracking is employed by fixating a tailored dental splint on the subject's upper jaw. However, producing such dental splints is cumbersome and exposes subjects to significant discomfort due to the required dental cast preparation. To catalyze the production of these custom-made splints, we propose a semi-automated workflow.By retrospectively digitizing dental casts of five subjects using a 3D laser scanner, we virtually graft the dental splints and, once visually analyzed and approved, they are fabricated by a 3D printer.This process increases subject comfort and reduces the preparation time.

## 1 Introduction

Magnetic resonance imaging (MRI) has become an important modality for medical diagnosis and neuroscientific research due to its non-invasive nature. The availability of enhanced contrast mechanisms and the increased signal-to-noise ratio (SNR) at higher field strengths promoted ultrahigh-field magnetic resonance imaging (UHF-MRI), enabling anatomical, vascular and functional imaging with much higher resolution [1]. Various problems arise from the relatively long scan time of typically several minutes for a single volume. Particularly at high resolution, data acquisition is sensitive to subject motion, which can induce artifacts and significantly degrade image quality. An effective correction of 3D rigid-body motion of the head can be achieved by using prospective motion correction (PMC) [2]. This method employs motion tracking to perform a real-time update of the MRI system's spatial encoding (gradients and frequencies) during data acquisition. In our current setup, 6 degrees of freedom (DOF) head movement is tracked with a single camera using a moiré pattern target.

Several fixation methods for the optical target, e.g. tape, clay or goggles, at different locations, e.g. between the eyes or on the forehead, have been analyzed. Even though PMC with these fixation methods might help to reduce strong motion artifacts and improve image quality, the stability and, thus, the accuracy is not suitable for ultrahigh resolution imaging [3]. As we attach the target to the subjects upper jaw using a custom-made dental splint, it is rigidly moving with



K.H. Maier-Hein et al. (Hrsg.), *Bildverarbeitung für die Medizin 2017*,
Informatik aktuell, DOI 10.1007/978-3-662-54345-0_45

the head. Hence, the tracked data represents the motion of the human brain, rendering these splints suitable for UHF-MRI [4]. The production of conventional dental splints (top image of Fig. 1(d)) takes several days. Consequently, subjects are invited a least twice: once for taking an imprint to form the dental cast and once to perform the actual study. If the dental splint does not perfectly fit, a third visit is necessary. This renders PMC impractical for studies with a large number of subjects. We suggest an optical scan to obtain a 3D model of the subjects teeth. The dental splint is created using an automated segmentation of the data and fabricated with a 3D printer at lower time effort and cost.

For this proof of concept study, we use digitized dental casts to graft dental splints. As intra-oral scanners are already available, we expect that the 3D information can be acquired directly from the subjects jaw for future studies, as described by Salmi et al. [5]. They create dental occlusal splints using surface extrusion of the acquired geometric mesh. Since computing offset surfaces is rather complicated, especially in highly curved regions as the teeth, artifacts might occur. Motivated by their approach, the contributions of this paper can be summarized as follows:

- a semi-automated approach for virtual dental splint identification,
- a volumetric method to graft artifact-free splints of arbitrary thickness, and
- a quick and cost-effective production of these dental splints.

## 2 Materials and methods

Since we aim to produce the splint and perform the actual MRI examination in only one visit, we simplify and catalyze the conventional process, i.e. make it less personnel-intensive, by proposing a new workflow (Fig. 1) that uses 3D printing. In the first step, we retrospectively digitize dental casts using a 3D laser scanner. Secondly, the region-of-interest (RoI) of the desired dental splint is determined and, thirdly, the digital model of the dental splint is generated and subject to quality assurance in form of visual inspection. Once approved, it is exported and, as fourth step, 3D printed. Each step of our workflow is subsequently detailed.

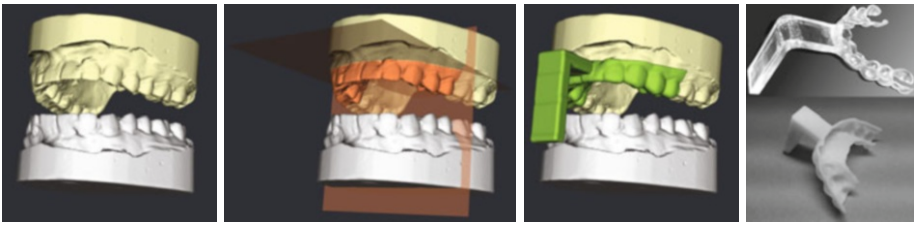

(a) Digitization (b) RoI Identification (c) Generation (d) Fabrication

**Fig. 1.** Our proposed workflow. (a) shows the digitized dental cast of the upper jaw (yellow) and the mirrored (white) as context below. The RoI of the dental splint is determined in (b) and the splint is generated in (c). The conventional dental splint is shown in the top image of (d) and our fabricated splint in the bottom image.

### 2.1 Dental cast digitization

The physical dental casts of the subjects' upper jaws have been digitized with a Minolta Vivid 910 / VI-910 non-contact 3D digitizer. The casts have been placed on a computer-controlled turntable and twelve scans with an angular turn of 30° between each have been acquired. In total, we recorded 24 scans per dental cast of five subjects, two full rotations from two different viewing angles to capture all details of the physical casts and reduce post-processing.

The registration and merging has been accomplished with the Polygon Editing Tool software from Minolta. The resulting 3D mesh of the cast is then imported into Autodesk MeshMixer for post-processing, i.e. closing holes and merging double surfaces. After removing minor artifacts, such as falsely joint teeth, the mesh is re-meshed to obtain a uniform distribution of triangles. Finally, the mesh is properly aligned to determine the RoI of the dental splint.

### 2.2 Region-of-Interest identification

After digitizing the 3D dental cast to obtain a 3D triangular mesh $\mathcal{M}_\triangle$, the RoI enclosing the dental splint has to be determined. Motivated by Kronfeld et al. [6], we define the RoI by automatically estimating two clipping planes (Fig. 1(b)).

Since the dental splint should optimally cover only teeth and not the gum, the first clipping plane should separate teeth from gum. We compute the mean curvature at all vertices of $\mathcal{M}_\triangle$, since it captures local changes. Kronfeld et al. [6] suggest to fit a plane to the vertices with a mean curvature value below $-0.3$, i.e. concave regions, for a good separation. By computing the full $3 \times 3$ covariance matrix of all vertices around the geometric centroid of $\mathcal{M}_\triangle$, the plane $\mathcal{T}$, referred to as transverse plane, is defined by the centroid $\boldsymbol{c}_\mathcal{T}$ and the direction with the largest eigenvalue. This plane splits the space into two half spaces $\mathcal{T}^+$ (superior) and $\mathcal{T}^-$ (inferior) according to the direction of its normal vector $\boldsymbol{n}_\mathcal{T}$ (superior). As the splint might not cover all teeth, the RoI has to be constrained further.

The second clipping plane is specified parallel to the $xz$-plane and referred to as coronal plane, denoted with $\mathcal{C}$. Again, this plane splits the space into two half spaces $\mathcal{C}^+$ (anterior) and $\mathcal{C}^-$ (posterior) depending on the direction of its normal vector $\boldsymbol{n}_\mathcal{C}$ (anterior). Initially, its centroid $\boldsymbol{c}_\mathcal{C}$ is set to $\boldsymbol{c}_\mathcal{T}$.

The RoI $\mathcal{R}$ of the dental splint is then the intersection of the inferior and anterior half spaces, denoted by $\mathcal{R} = \mathcal{T}^- \cap \mathcal{C}^+$. The geometric preview $\mathcal{P}_\triangle$ of the dental splint is obtained as the intersection of $\mathcal{M}_\triangle$ with $\mathcal{R}$, denoted as $\mathcal{P}_\triangle = \mathcal{M}_\triangle \cap \mathcal{R}$. Both planes can be manually adjusted by moving their centroids along their normal vectors, while simultaneously updating $\mathcal{P}_\triangle$. This facilitates the user a visual assessment of the dental splint before generation and fabrication.

### 2.3 Dental splint generation

Once the RoI of the dental splint is specified, we compute the geometry of the splint by using the digitized dental cast $\mathcal{M}_\triangle$. Therefore, we voxelize $\mathcal{M}_\triangle$ and then, subsequently, apply several 3D image processing operations.

Voxelizing a mesh requires specifying the spacing, i.e. the number of voxels per millimeter, of the target volumetric dataset. Since the initial bounds of the volumetric dataset tightly fit $\mathcal{M}_{\triangle}$, we enlarge the dataset inferior and anterior. This prevents the dental splint from exceeding the dataset due to its thickness and attached tracking construction. As result, we obtain a volumetric representation $\mathcal{M}_{\boxplus}$ approximating the geometric representation $\mathcal{M}_{\triangle}$, denoted as $\mathcal{M}_{\triangle} \mapsto \mathcal{M}_{\boxplus}$. Within the volumetric dataset, the dental cast $\mathcal{M}_{\boxplus}$ is marked as foreground (value of 1) and all other voxels as background (value of 0).

We then attach, i.e. mark as foreground, an L-shaped volumetric tracking construction $\mathcal{L}_{\boxplus}$ (Fig. 1(c)) to $\mathcal{M}_{\boxplus}$ at the most anterior part of $\mathcal{R}$, leading to the volumetric input $\mathcal{I}_{\boxplus} = \mathcal{M}_{\boxplus} \cup \mathcal{L}_{\boxplus}$. Subsequently, we perform 3D morphologic dilation on the foreground with a spherical structuring element (SE) of such a radius in voxels that it represents the desired thickness of the splint in millimeters. Since all voxels, including the interior, of $\mathcal{I}_{\boxplus}$ are marked as foreground, this operation creates a thick layer around $\mathcal{I}_{\boxplus}$ denoted as $\mathcal{I}_{\boxplus}^{\oplus} = \mathcal{I}_{\boxplus} \oplus \text{SE}$. We then subtract the original volumetric input from the dilated one, leaving only the outer shell behind, denoted as $\overline{\mathcal{I}}_{\boxplus} = \mathcal{I}_{\boxplus}^{\oplus} - \mathcal{I}_{\boxplus}$. The voxels of the dental splint are computed by the intersection of $\mathcal{R}$ with the volumetric outer shell $\overline{\mathcal{I}}_{\boxplus}$, denoted as $\mathcal{S}_{\boxplus} = \overline{\mathcal{I}}_{\boxplus} \cap \mathcal{R} = \{\forall \boldsymbol{v} \in \overline{\mathcal{I}}_{\boxplus} | (\boldsymbol{v} - \boldsymbol{c}_{\mathcal{T}}) \cdot \boldsymbol{n}_{\mathcal{T}} < 0 \wedge (\boldsymbol{v} - \boldsymbol{c}_{\mathcal{C}}) \cdot \boldsymbol{n}_{\mathcal{C}} > 0\}$. However, this leads to one-voxel thin parts that might be problematic for 3D printing. To remove these remnants and boundary noise, a morphological opening is applied on $\mathcal{S}_{\boxplus}$ using a spherical SE with a radius of one voxel, denoted as $\mathcal{S}_{\boxplus}^{\circ} = \mathcal{S}_{\boxplus} \circ \text{SE}$.

To fabricate the volumetric dental splint, it is converted back to a geometric representation $\mathcal{S}_{\boxplus}^{\circ} \mapsto \mathcal{S}_{\triangle}$, using marching cubes. Finally, we smooth the obtained geometric representation using an algorithm that is based on the work of Taubin [7] and export the dental splint as STL file that is sent to the 3D printer.

### 2.4 Dental splint fabrication

The dental splint is additively manufactured by a Stratasys Mojo 3D printer using the FDM Thermoplastics ABSplus with soluble support material. Since the dental splints should accurately adapt to the teeth, we print them with their tracking constructions facing downward, as printing support material inside the splints might result in unwanted small remnants even after being washed out.

## 3 Results

We automatically manufactured dental splints for five subjects (Fig. 2), voxelized with a spacing of 0.2, i.e. five voxels per millimeter, and expanded 3 cm inferior and anterior. The splints and tracking constructions are 1 mm thick and the L-shaped tracker spans $10 \times 20 \times 3$ mm anterior and $10 \times 3 \times 30$ mm inferior. We present (Fig. 2) the digitized dental casts and splints as well as the fabricated dental cast and splints (two hours 3D printing time on average, excluding cast digitization). Our workflow is implemented in C++, using VTK and ITK, and executed on an Intel i7 at 4 GHz with 16 GB RAM and an Nvidia GTX 560 Ti. Our automated dental splint creation takes on average two minutes.

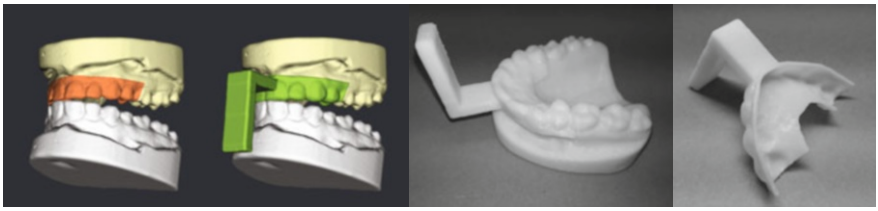

(a) Subject 1: Easy case. Transverse plane well estimated.

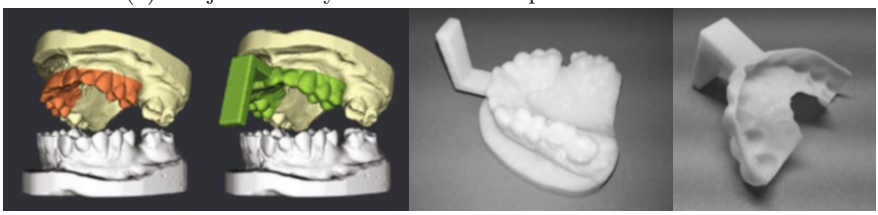

(b) Subject 2: Hard case. Highly varying teeth. Splint overflows to gum.

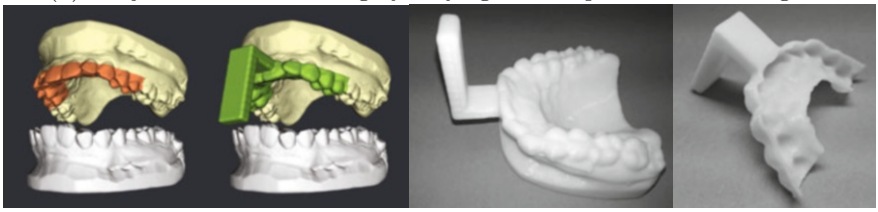

(c) Subject 3: Medium case. Teeth slightly varying. Splint overflows to gum.

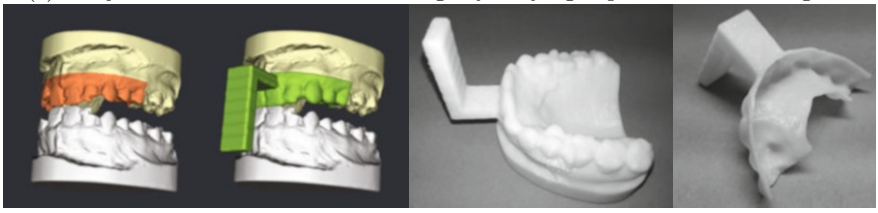

(d) Subject 4: Hard case. Damaged dental cast. Splint highly overflowing to gum.

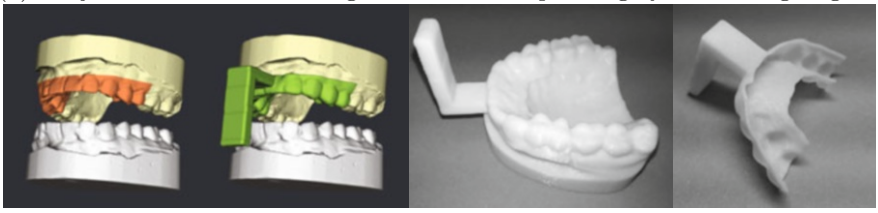

(e) Subject 5: Easy case. Transverse plane well estimated.

**Fig. 2.** Automatically generated results of our approach, without any user adjustments of the transverse and coronal planes. To serve as context, we display the upper jaw (yellow) transversely mirrored as lower jaw (white). For each subject, we present, from left to right, the digitized dental cast, the generated dental splint, the fabricated dental splint alone and attached to the fabricated cast.

## 4 Discussion

To conclude, we presented an approach for fabricating dental splint using digitized 3D dental casts. Our proposed workflow streamlines as well as standardizes the production of tracking constructions for PMC in UHF-MRI. This does not only facilitate a larger population to access this rather recent acquisition modality, but also catalyzes this process.

As future work, we plan to investigate more flexible materials, as described by Bickel et al. [8], compared to the stiff splints as currently fabricated. Combined with the teeth segmentation presented by Kronfeld et al. [6] or Wu et al. [9], this would create a dental splint that might snap to the teeth. The visual assessment of the splint geometry before the fabrication can be improved using visual analytics approaches such as proposed by Schmidt et al. [10].

**Acknowledgement.** The dental casts were created in the local department of oral and maxillofacial surgery for five subjects (three male and two female, between 26 and 43 years of age) from alginate impressions. The study was performed with the approval of the ethics committee of the Otto-von-Guericke University Magdeburg, Germany. The work of this paper is partly funded by the Federal Ministry of Education and Research within the Forschungscampus STIMULATE (grant no. 13GW0095A) and the NIH (grant no. R01DA021146).

## References

1. Balchandani P, Naidich TP. Ultra-high-field MR neuro-imaging. AJNR Am J Neuroradiol. 2015;36(7):1204–15.
2. Godenschweger F, Kägebein U, Stucht D, et al. Motion correction in MRI of the brain. Phys Med Biol. 2016;61(5):32–56.
3. Herbst M, Lovell-Smith C, Haeublein B, et al. On the robustness of prospective motion correction for clinical routine. Proc 21st Sci Meet. 2013; p. 3766.
4. Stucht D, Danishad KA, Schulze P, et al. Highest resolution in vivo human brain MRI using prospective motion correction. PloS one. 2015;10(7):e0133921.
5. Salmi M, Paloheimo KS, Tuomi J, et al. A digital process for additive manufacturing of occlusal splints: a clinical pilot study. J R Society Interface. 2013;10(84):20130203.
6. Kronfeld T, Brunner D, Brunnett G. Snake-based segmentation of teeth from virtual dental casts. Comput Aided Des Appl. 2010;7(2):221–33.
7. Taubin G. A signal processing approach to fair surface design. Proc ACM SIGGRAPH. 1995; p. 351–8.
8. Bickel B, Bächer M, Otaduy MA, et al. Design and fabrication of materials with desired deformation behavior. ACM Trans Graph. 2013;29(4):63:1–10.
9. Wu K, Chen L, Li J, et al. Tooth segmentation on dental meshes using morphologic skeleton. Comput Graph. 2013;38(1):199–211.
10. Schmidt J, Preiner R, Auzinger T, et al. YMCA – Your mesh comparison application. Proc IEEE VAST. 2014; p. 153–62.